Cement and Concrete Composites 134 (2022) 104814

Contents lists available at ScienceDirect

Cement and Concrete Composites

journal homepage: www.elsevier.com/locate/cemconcomp

Mechanical anisotropy evaluation and bonding properties of 3D-printable construction and demolition waste-based geopolymer mortars

Nazim Cagatay Demiral [a,b], Mehmet Ozkan Ekinci [a,c], Oguzhan Sahin [d], Huseyin Ilcan [a,e], Anil Kul [a,e], Gurkan Yildirim [e], Mustafa Sahmaran [e,*]

[a] Institute of Science, Hacettepe University, Beytepe, Ankara, Turkey
[b] Department of Civil Engineering, Bilecik Seyh Edebali University, Bilecik, Turkey
[c] Limak Cement Co., Research and Development Center, Ankara, Turkey
[d] Department of Civil Engineering, Ankara University, Ankara, Turkey
[e] Department of Civil Engineering, Hacettepe University, Beytepe, Ankara, Turkey

ARTICLE INFO

Keywords:
3D-printing
Construction and demolition waste (CDW)
Geopolymer
Anisotropy
Alkaline content
Bond strength

ABSTRACT

This work aims at evaluating the anisotropy (direction-dependency) in terms of mechanical performance and bonding properties of entirely construction and demolition waste (CDW)-based geopolymer mortars fabricated by 3D-additive manufacturing (3D-AM) technique. In the study, a combination of hollow brick (HB), red clay brick (RCB), roof tile (RT), concrete waste (CW) and glass waste (GW) obtained from various demolition sites and different combinations of alkaline activators including sodium hydroxide (NaOH) and calcium hydroxide ($Ca(OH)_2$) were used for geopolymerization. CW was also used as fine aggregate in geopolymer mortar production. Specimens were subjected to ambient curing conditions until testing ages. Direction-dependent mechanical performance of printed specimens was evaluated at 7-, 28- and 90-day via compressive strength test in three different loading directions of perpendicular, parallel, and lateral to the printing path and flexural strength test in two different loading directions of perpendicular and lateral to the printing path. Moreover, bond strength between the consecutive printed layers were tested through direct and splitting tensile strength tests at the end of 7-, 28- and 90-day ambient curing and used to compare the directional performance of tested mixtures. In addition, compressive and flexural strength test results of printed specimens were compared with those of conventional mold-casted specimens. Results showed that alkaline activator content affects the mechanical properties considerably. According to compressive and flexural strength test results, 3D-printed geopolymer mortar specimens have anisotropic behavior and the bond performance between consecutive layers is one of the main influencing parameters for the anisotropic behavior of 3D-printed structures. However, perpendicular-loaded 3D-printed specimens showed similar or slightly better performance compared to the mold-casted ones, indicating that the bond zone had little influence on the performance of specimens loaded in perpendicular loading direction. This study pointed out that the anisotropic performance of printed structures can be diminished with the enhanced bond adhesion between consecutive layers and the adhesion can be improved by optimizing the rheological properties and matrix performance of the mixtures.

1. Introduction

In regard to different essential properties of construction industry such as higher speed of construction, design flexibility, and material and energy efficiency, the current technologies are at their limits. To shift beyond those boundaries, automation is expected to provide a striking enhancement. Although the integration of automation systems into the construction sector dates back to 1960s, progress has not been made as rapidly as in different fields (*e.g.*, automotive sector) [1]. In the last few years, the most revolutionary development in integrating automation systems into the construction industry has been made with the use of 3-dimensional concrete printing (3DCP) systems in building construction. In the current situation, where construction companies are looking for new ways to increase efficiency and reduce costs in construction, 3DCP can lead to numerous economic and environmental benefits compared to traditional methods [2]. The main benefits that 3DCP

* Corresponding author.
E-mail address: sahmaran@hacettepe.edu.tr (M. Sahmaran).

https://doi.org/10.1016/j.cemconcomp.2022.104814
Received 26 April 2022; Received in revised form 11 October 2022; Accepted 12 October 2022
Available online 17 October 2022

technique may bring are the reduction in the production-related errors, production time, risks of occupational safety, and cost [3]. Specifically, compared to traditional methods, 3DCP provides significant advantages in decreasing the formwork costs, which have an approximate share of 35–60% in the total construction costs [4,5]. 3DCP method can also significantly reduce the environmental impact caused by traditional construction methods [6]. Another remarkable benefit of 3DCP technique is the minimization of amount of post-production waste by enabling a production process in which construction waste is managed correctly, and material consumption is optimized [7,8]. Taking all these advantages into account, the integration of the 3DCP technique into the construction industry can play an essential role in the changing world [9].

Measures for the problems related to the Portland cement production and construction and demolition waste (CDW) generation, which are two interdependent issues, have a key role in eliminating the negative burden of construction industry on the environment, economy, and society. Energy- and carbon-intensive production procedure of Portland cement together with the inability to reduce the embodied carbon and improper disposal of CDW are serious problems, which require urgent and proper tackling [10,11]. Global cement production has experienced an extreme increase from 0.94 billion tons (in 1970) to 4.1 billion tons (in 2018) [12]. Moreover, it is expected that 45% more cement will be manufactured by 2050 if alternative binders are not proposed [13]. Meanwhile, CDW-related reports indicate that roughly 570 million tons of CDW were produced in the United States in 2017 [14] and the volume of CDW produced in the European Union is approximately 35% of the total waste production, that is, over 700 million tons per year [15]. Reuse rates of CDW approach 80% in some countries, such as Germany, Denmark, and the Netherlands, whereas the same rates for the remaining countries are on average less than 30% [11,16]. Even so, the majority of CDWs are used for non-structural filling purposes for road pavements or pathways with no added value [17–19]. Under such circumstances, development of a holistic solution that can eliminate the unbearable burden of cement production and CDW generation and help forming a sustainable circular economy in the construction industry, can possibly be proposed through the geopolymer technology (via reaction between aluminosilicate source materials [*e.g.*, CDWs] and alkaline activators).

In recent years, limited number of studies have been carried out to adapt geopolymers, as environmentally friendly construction materials, into 3DCP technology to combine materials- and production-related breakthroughs. In one of such studies, Chougan et al. [20] investigated the 3D printability of geopolymer binders produced by activating fly ash, granulated blast furnace slag, silica fume precursors with sodium hydroxide (NaOH) and sodium silicate (Na_2SiO_3) as the alkaline activators. Rheological, mechanical and buildability properties of the 3D-printed mixtures were investigated. Although the majority of the mixtures were found to show anisotropic behavior according to Young's Modulus, that is, mechanical performance was direction-dependent; no detailed research has been performed to evaluate whether this behavior was negligible in 3D-printed geopolymers. In another study, Panda et al. [21] investigated the mechanical properties and anisotropic behavior of fly ash-based 3D-printed geopolymers. In this study, compressive strength tests for three different directions and flexural strength tests for two different directions were performed on 3D-printed specimens, and the results were compared with the mold-casted specimens. Compared to mold-casted specimens, 3D-printed specimens had 5% less compressive strength under perpendicular and parallel loading and 2% higher under lateral loading. These findings revealed that the 3D-printed geopolymer exhibits anisotropic behavior depending on the loading directions. In addition, the bond strength was determined by performing direct tensile tests on the 3D-printed specimens and the maximum bond strength was reported to be 1.4 MPa. Nematollahi et al. [22] investigated the effect of polypropylene fibers on the fresh and hardened properties of 3D-printed fly ash-based geopolymer mortars. Compressive strength in three different loading directions and flexural strength in two different loading directions were studied in addition to the workability and extrudability of the mortars. The results showed that fiber reinforcement had a positive effect on the compressive strength only for the specimens loaded in perpendicular (perpendicular to the printing direction) loading direction. Also, according to their compressive strength test results depending on the loading directions, the maximum difference between perpendicular and lateral loading was reported to be 20.8 MPa. Bong et al. [23] investigated the buildability and mechanical performance of slag and fly ash-based geopolymers activated by Na_2SiO_3 with different dosages and reported that compressive strength variation depending on the loading direction was 23% in three different directions. In a different work performed by Panda et al. [24], fresh and hardened properties of geopolymers produced from fly ash, granulated blast furnace slag and silica fume were investigated. As a result of the compressive strength tests performed only in the perpendicular direction to examine the compressive strengths of 3D-printed and mold-casted geopolymers, it has been reported that the influence of the production technique on the compressive strength is negligible. This study reported that compressive strength results of the 3D-printed and mold-casted specimens were 18.4 MPa and 16.2 MPa, respectively. However, in another study of Panda et al. [25], it was emphasized that fly ash-based geopolymers produced with 3DCP technology showed directional variations in their mechanical properties. As a result of flexural strength tests for three different loading directions, the maximum difference between direction-dependent performances was reported to be ~50%. Nematollahi et al. [26] performed compression tests in three different directions and flexural tests in two different directions on Class F fly ash-based geopolymer specimens and measured the interlayer bond strength between the 3D-printed layers. Results showed that the compressive strength of the specimen under parallel loading was 50% higher than that of the specimen under lateral loading. For flexural strength results, it was reported that the specimens tested under lateral loading showed 6.5% higher strength than that recorded under perpendicular loading. Interlayer bond strength of geopolymer mixtures were obtained to be between 2.33 and 3.03 MPa. In another study, Nematollahi et al. [27] performed compressive strength tests in three different directions, flexural tests in two different directions and time-dependent (2 and 15 min delay after the first layer when printing two layers) interlayer bond strength tests on 3D-printed geopolymers produced by using fly ash and granulated blast furnace slag. As a result of the compressive strength tests, the specimens loaded in parallel to the printing path were 72% higher than those of loaded in lateral. On the other hand, for flexural strength, 65% of the lateral loading was obtained under perpendicular loading. Maximum of 1.3 MPa interlayer bond strength was also reported. In the study of Muthukrishnan et al. [28], compressive and flexural strength tests in three different directions were applied to the fly ash and granulated blast furnace slag-based geopolymer specimens. According to 28-day test results, compressive and flexural strength test specimens loaded in parallel direction showed 28% and 56% higher strength than those loaded in perpendicular direction, respectively. In the above-detailed existing studies related to 3DCP, different mechanical performances obtained in different loading directions are generally explained by the anisotropic property caused due to weak bonding region between the layers due to the nature of 3D printing process.

In general sense, literature studies related to 3DCP process and performance of 3D-printed structures showed that due to layer-by-layer deposition approach of 3D-AM method, the mechanical performance of the printed specimens can be influenced by the direction of loading and the interlayer bond (adhesion) between the two consecutive layers. Therefore, anisotropic mechanical performance of the layer-by-layer manufactured structures and the interlayer bond strength between the two printed consecutive layers should be evaluated to determine the printing compatibility of the mixtures at hardened state. Moreover, these need to be assured for geopolymer materials manufactured with

different types of precursors, as opposed to vast majority of literature focusing on the use of mainstream pozzolanic materials such as fly ash and ground granulated blast furnace slag, which are highly demanded and not regarded as waste anymore by many. Considering the existing divergency in literature and deficiency of studies regarding the performance of 3D-printed CDW-based geopolymer mortars, the direction-dependent mechanical and bond strength performance of entirely CDW-based geopolymer mortars was mainly focused herein. Geopolymer mortars were produced by using different components of CDW-based materials, including hollow brick (HB), red clay brick (RCB), roof tile (RT), concrete waste (CW) and glass waste (GW). Geopolymer binders were incorporated with CW-based fine aggregates to increase the waste upcycling potential and reduce the need for clean raw materials. To activate the precursors, NaOH and $Ca(OH)_2$ were used in different combinations, as the alkaline activators. Direction-dependent mechanical performances of CDW-based geopolymer mortars were assessed via compressive strength tests in three different directions and 3-point flexural tests in two different directions on the 3D-printed specimens. In addition, direct tensile and splitting tensile tests were performed to determine the bond strength. Performance characteristics of 3DCP technique were also evaluated by comparing 3D-printed specimens with the mold-casted specimens. Aside from the influences of the manufacturing technique, the effects of different alkaline activator types and combinations on the mechanical properties were examined.

2. Experimental program

2.1. Materials

CDW-based materials including HB, RCB, RT, GW and CW, collected from variety of selective demolition activities performed in Turkey, were used as precursors in the production of geopolymer mortars. All these waste-originated materials were first crushed individually with a jaw crusher to reduce the size and then milled for 60 min in a ball mill to obtain their powder forms. After milling process, X-ray fluorescence (XRF) analysis with the wavelength of 0.1–50 Å and laser diffraction technique with the size range sensitivity of 0.02–2000 μm were performed on oven-dried powders taken from different regions of powder batches to determine the oxide compositions (Table 1) and particle size distribution (PSD) (Fig. 1) of the precursors, respectively. As seen in Table 1, SiO_2, Al_2O_3 and Fe_2O_3, which are fundamentally important oxides for geopolymerization process [29], were found in high quantities in clay-originated materials (HB, RCB, and RT). In addition to the clay-originated CDW-based precursors, GW and CW precursors had high percentages of SiO_2, Na_2O and CaO.

As seen in Fig. 1, at the end of the crushing and milling procedures, powdery precursors had different PSDs. HB, RCB, and RT had similar PSD, while CW and GW had coarser particle size distributions compared to the others. Approximately 90–95% of HB, RCB, and RT were finer than 40 μm and the amount of CW finer than 40 μm was ~80%. Among all precursors, GW was with the coarsest grain size; only 60% remained below 40 μm. Differences in the PSDs of the powdery precursors after the same milling process was most probably related to the differences in the grindability index, hardness, density and pore structure of the materials.

Table 1
Chemical compositions and specific gravity of CDW-based precursors.

Oxides %	HB	RCB	RT	GW	CW
SiO_2	39.7	41.7	42.6	66.5	31.6
Al_2O_3	13.8	17.3	15.0	0.9	4.8
Fe_2O_3	11.8	11.3	11.6	0.3	3.5
CaO	11.6	7.7	10.7	10.0	31.3
Na_2O	1.5	1.2	1.6	13.6	0.45
MgO	6.5	6.5	6.3	3.9	5.1
SO_3	3.4	1.4	0.7	0.2	0.9
K_2O	1.6	2.7	1.6	0.2	0.7
TiO_2	1.7	1.6	1.8	0.1	0.2
P_2O_5	0.3	0.3	0.3	0.0	0.1
Cr_2O_3	0.1	0.1	0.1	0.0	0.1
Mn_2O_3	0.2	0.2	0.2	0.0	0.1
Loss on ignition	7.8	8.0	7.5	4.3	21.1
Specific gravity	2.89	2.81	2.88	2.51	2.68

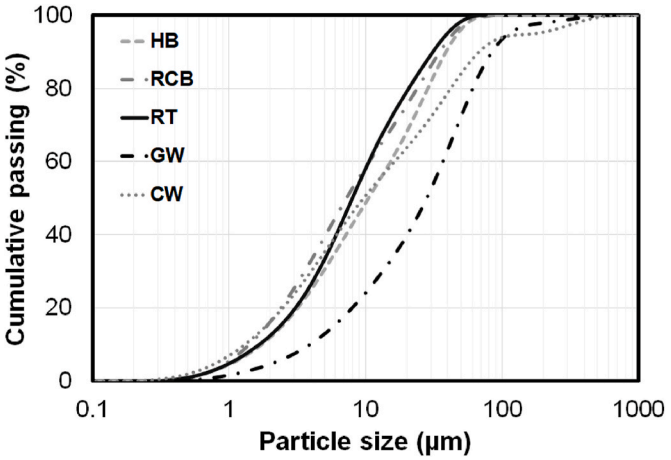

Fig. 1. Particle size distributions of the precursors.

Instead of natural aggregates, fine recycled concrete aggregates (RCA) obtained by crushing waste concrete rubbles was used to produce geopolymer mortars. Considering the 3D-printing application procedures, maximum particle size of the aggregates was limited to 2 mm for each mixture. At first, a jaw crusher with a 2 mm opening was used to reduce the size of the concrete waste rubbles. Then, crushed RCA were sieved by using a 2-mm sieve. Obtained RCA from the concrete rubbles were directly used in geopolymer mortar mixtures without applying any kind of treatment to enhance their mechanical and durability properties.

To activate CDW-based precursors, NaOH and $Ca(OH)_2$ were used as the alkaline activators, in different usage rates and combinations, as detailed in the following section. NaOH was solid and in flake form with 98% purity level and the $Ca(OH)_2$ was in powder form and had a purity level of 87%. More detailed information regarding the alkaline activators can be found in the previous works of the authors [30,31].

2.2. Mixture proportions

Proportions of the geopolymer mortar mixtures produced in this study were designed considering the extensive studies carried out by the authors. In this regard, a dry base mixture was designed to have 80% brick-based materials (HB, RCB and RT), 10% GW and 10% CW. Since the physical and chemical properties of RCB, RT, and HB were similar, brick-based material content was chosen to have equal percentages in the mixture (~26.67% for each). Usage rates of GW and CW were limited to 10% by considering the Si/Al balance of the geopolymer systems. Aggregate to binder ratio of 0.35 and water to binder ratio of 0.33 (by weight) were used for each mixture.

To investigate the effect of activators on the bond strength and anisotropic behavior of the developed geopolymer mortars, 10 M and 12.5 M NaOH and 0, 4 and 8% $Ca(OH)_2$ (by weight of precursor) were used solely and in binary combinations. These ranges and combinations were designed by considering previous studies of the authors [30,31]. As increased NaOH molarity leads to higher viscosity, thereby lower printability performance, NaOH molarity was limited to 12.5 M. Likewise, increased usage rates of $Ca(OH)_2$ led to increased amounts of geopolymerization products and solid content, hence decreased flowability. Thus, usage rate of $Ca(OH)_2$ was limited to maximum 8%, by the weight of binder material. Designed CDW-based geopolymer mortars without additional chemical admixtures other than the alkaline activators performed satisfactorily in terms of shape retention, and

extrudability during 3D-AM process. Details of the designed mixtures were presented in Table 2 alongside with the flowability indexes. The flowability index given in Table 2 is an indicator of the fresh properties of the materials and an increment in this index means an increment in flowability and vice versa.

2.3. Mixture preparation

Mixture preparations were started with the preparation of NaOH solutions. To obtain NaOH solutions with different molar concentrations, required amounts of solid NaOH for a desired molar concentration was dissolved in tap water. Then, to avoid the heat-related effects as a result of the exothermic reactions between the NaOH and water, prepared solutions were kept in the laboratory medium until reaching constant room temperature. Different from NaOH solution, powdery Ca $(OH)_2$ was directly added to the dry mixtures. After preparing the NaOH solution, the mixing process was started by mixing all powdery ingredients (*i.e.*, CDW-based precursors, fine recycled aggregate, and Ca $(OH)_2$ [if available for a given mixture]) for 2 min in a pan-type mixer. Then, NaOH solution was gradually added to the mixer, and the mixing was continued for 5 min to ensure that the solution was evenly mixed with the dry mixture.

2.4. Specimen preparation and curing

Both 3D-printed and mold-casted geopolymer mortar specimens were produced to examine the effects of manufacturing methods on the mechanical properties of the mixtures. After the completion of mixing, prismatic specimens with dimensions of 4 × 4 × 16 cm were prepared for each mixture by pouring mixtures into the pre-oiled molds in two stages (Fig. 2a). Vibration was applied to the molds by a vibration table in both stages of pouring to prevent the formation of air voids. Casted mixtures were kept under laboratory conditions for 24 h and then extracted from their molds and cured until the testing ages under ambient conditions (temperature of 23 ± 2 °C and relative humidity of 50 ± 5%).

For 3D-printing applications, a lab-scale gantry system 3D-printer, details of which can be found in authors' recent work [31], was used. 3D-printer used consisted of a mortar pump, transmission pipe, CNC router and control panel and was with the printing volume of 100 × 100 × 40 cm^3 (width × length × height). Mixtures were loaded into the pump container of the 3D-printer and printed by using a rectangular nozzle and G-Code-based 3D-printing path design. Although the parameters related to 3D-printing process have clear effects on the ultimate performance of the printed structure, in this study, process-related parameters were kept constant for each mixture since the main focus was on materials-related parameters. The nozzle speed was set at 60 mm/s. Two-layered filaments with the length of 80 cm (chosen by considering the limitation of 3D-printer) and cross-section of 40 × 40 mm were printed uniformly side by side without any breaking time between the consecutive layers while printing. Immediately after the printing, 40 × 40 × 40 mm cubic and 40 × 40 × 160 mm prismatic specimens (Fig. 2b) were carefully extracted from these fresh

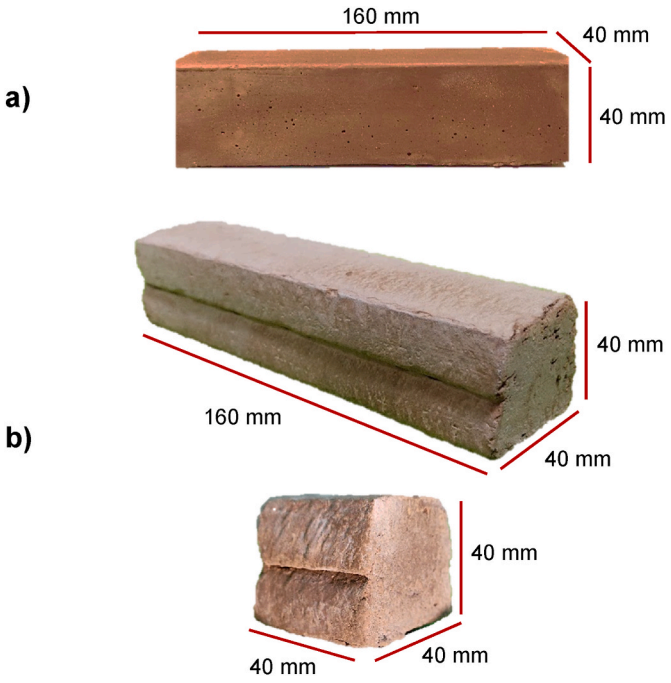

Fig. 2. Representative images showing the details of test specimens: a) Prismatic mold-casted specimen, b) prismatic and cubic 3D-printed specimens.

longitudinal two-layered filaments by cutting them with thin fishing line. Cubic and prismatic specimens were kept on the printing table until hardening and then moved to the curing medium. The curing process was carried out under ambient conditions to accurately simulate the field application conditions of the 3D-printing process. Within this context, printed specimens were also cured under laboratory conditions (23 ± 2 °C) until the testing ages of 7, 28 and 90 days.

2.5. Testing

2.5.1. Flexural strength test

3-point flexural strength test was performed on prismatic mold-casted and 3D-printed specimens in two directions including perpendicular and lateral to the printing direction (Fig. 3) by using a universal testing machine at a crosshead speed of 0.05 mm/s to evaluate the direction-dependent behavior of 3D-printed specimens and manufacturing method-related flexural performance differences. Flexural strength of the specimens was calculated by using the following formula:

$$\sigma_f = \frac{3F_{max}L}{2bh^2}$$

where, F_{max} is the maximum load applied; L is the span length, b is the thickness of the specimen; h is the height of the specimen. A minimum of six replicates were used for each case (*e.g.*, mixture proportion, loading

Table 2
Proportions of geopolymer mortar mixtures.

Alkaline activators				CDW-based precursors (g)					RCA (g)	W/B	Flowability index [30]
NaOH		$Ca(OH)_2$		(1000 g)							
Molarity (M)	Amount (g)	Rate (%)	Amount (g)	HB	RCB	RT	CW	GW			
10	132	0	0	266.7	266.7	266.7	100	100	350	0.33	1.25
		4	40								0.77
		8	80								0.56
12.5	165	0	0								1.02
		4	40								0.56
		8	80								0.44

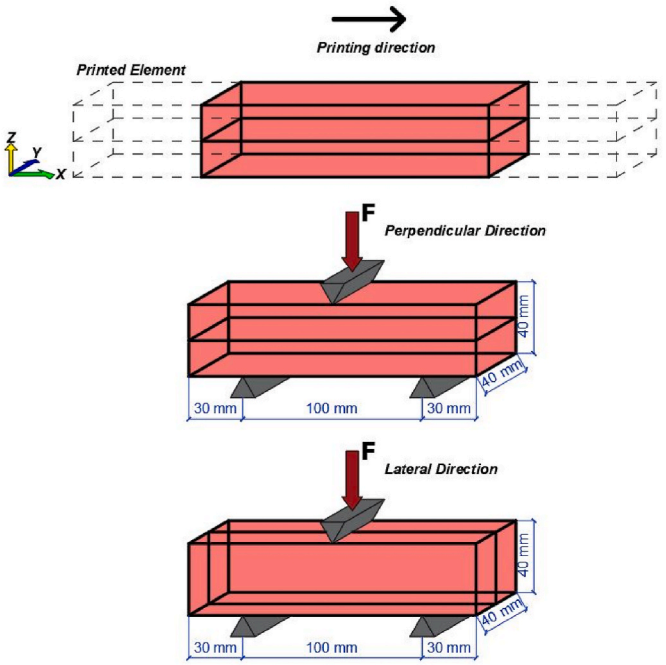

Fig. 3. Schematic representation of the flexural strength test.

direction, testing age etc.) and the results were averaged. Before testing, the b and h values of each specimen were measured to be more precise about the results.

2.5.2. Compressive strength test

Compressive strength tests were carried out on the mold-casted and 3D-printed specimens by using hydraulic testing machine with loading rate of 0.9 kN/s 3D-printed cubic specimens were subjected to compressive loading in three different directions, including perpendicular, parallel and lateral to the printing direction (Fig. 4), to evaluate anisotropy in terms of compressive strength measurements. For the compressive strength tests of mold-casted specimens, the pieces broken from the prismatic casted specimens used under flexure were used. To keep the compression area equal for each specimen, 40 × 40 mm steel plates were placed on the compression areas of the specimens. At least six replicates of each specimen were tested for each case (*e.g.*, mixture content, loading direction, testing age etc.) and the strength results were averaged.

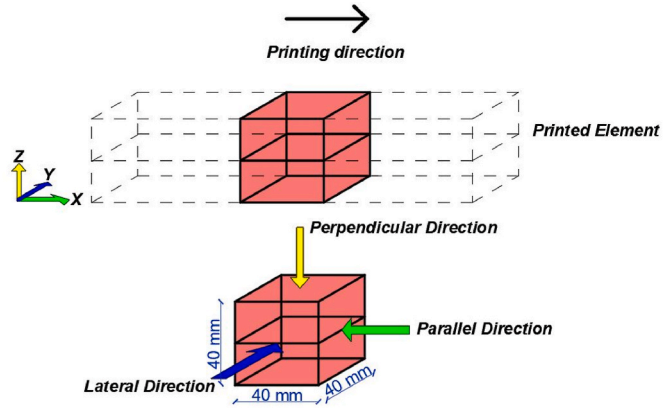

Fig. 4. Schematic representation of compressive strength test for three different loading directions.

2.5.3. Interlayer bond strength

To test the interlayer bond strength between 3D-printed layers, splitting tensile test following ASTM C496 [32] and direct tensile strength test inspired by Nematollahi et al. [26] were performed on 40-mm 3D-printed cubic specimens. For the splitting tensile test, specimens were placed between the compression plates and cylindrical metal rods were placed at the joint of two consecutive layers (Fig. 5a). Compressive stress was applied on the rods and the maximum force value required to split the layers from each other was determined. By using the obtained force value, splitting tensile strength was calculated according to Timoshenko [33] formula below:

$$\sigma_{ST} = \frac{2P_c}{\pi bh}$$

where, σ_{ST} is the splitting tensile strength, P_c is the magnitude of the splitting load, b is the width of the specimen and h is the height of the specimen.

For the direct tensile test, T-shaped steel profiles were firstly glued to the 40-mm printed cubic specimens 4 days before the testing day with epoxy-based adhesive. Epoxy-based adhesive used had enough adhesion strength (>3 MPa on concrete surface, >3.5 MPa on steel surface) to ensure adhesion between the plate and specimen so that there was no failure observed due to epoxy-based adhesive related problems during testing. On the day of testing, T-profiles glued to the specimens were carefully connected to single-hole metal plate with a pintle chain link to avoid any eccentricity during testing. Single-hole metal plates were fixed into the jaws of the tension machine and direct tensile stress was applied to the specimen (Fig. 5b). The direct tensile strength values of the 3D-printed specimens were found by dividing the failure load to the area under tension loading. For both splitting and direct tensile strength tests, at least six replicates of each specimen were tested for each curing age and strength results were averaged.

3. Results and discussion

3.1. Compressive strength

Mechanical performance of the 3D-printed specimens including compressive strength can vary with the loading direction since the 3D-printing process is a production method based on adding layer upon layer of material, resulting in interlayer bonding (adhesion) zone between consecutive printed layers. Mechanical properties of the bond interface of layers are relatively weaker than the core region of consecutive layers; thereby, a performance dependency, termed as anisotropy, emerges due to the loading and printing direction [34]. Therefore, to assess the anisotropic mechanical performance of layer-by-layer produced specimens and compare the effects of the manufacturing process on the mechanical performance of CDW-based geopolymer mortars, compressive strength tests were performed both on the printed (for three different loading directions including perpendicular, parallel, and lateral to printing direction) and mold-casted specimens.

The average compressive strength results of 7-, 28- and 90-day-old geopolymer mortars produced by the single use of NaOH and combination of NaOH–$Ca(OH)_2$ are presented in Fig. 6. The results of printed specimens reveal that independent of the other mixing parameters and loading conditions, the mechanical performances of the specimens show a continuous improvement trend due to the continuation of geopolymerization reactions in the maturing matrix. At the end of 90-day, maximum compressive strength results recorded for the mold-casted, perpendicular-, parallel- and lateral-loaded printed specimens were 20.5 MPa [10 M NaOH – 8% $Ca(OH)_2$], 21.5 MPa [10 M NaOH – 4% $Ca(OH)_2$], 19.9 MPa [10 M NaOH – 4% $Ca(OH)_2$] and, 17.5 MPa [10 M NaOH – 8% $Ca(OH)_2$], respectively. In general, the findings indicate that printed specimens exhibit comparable compressive strengths to the

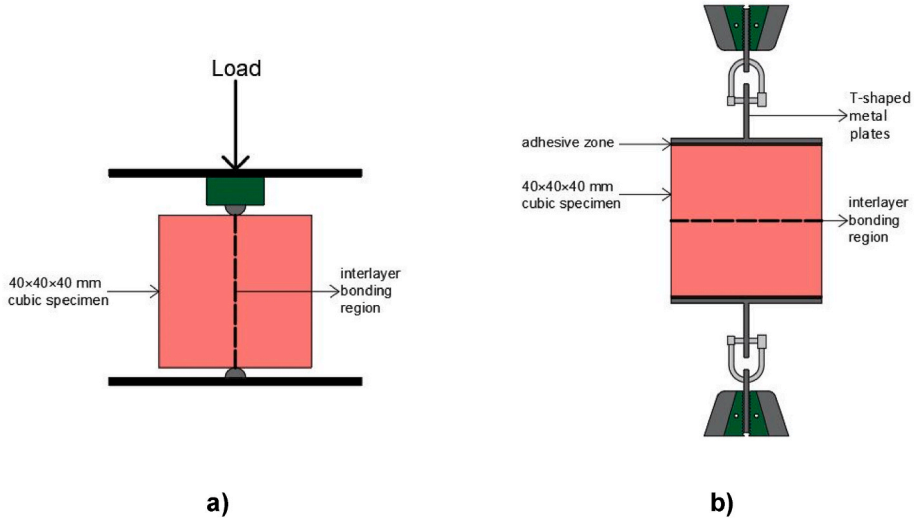

Fig. 5. Schematic representation of a) splitting tensile strength and b) direct tensile strength test.

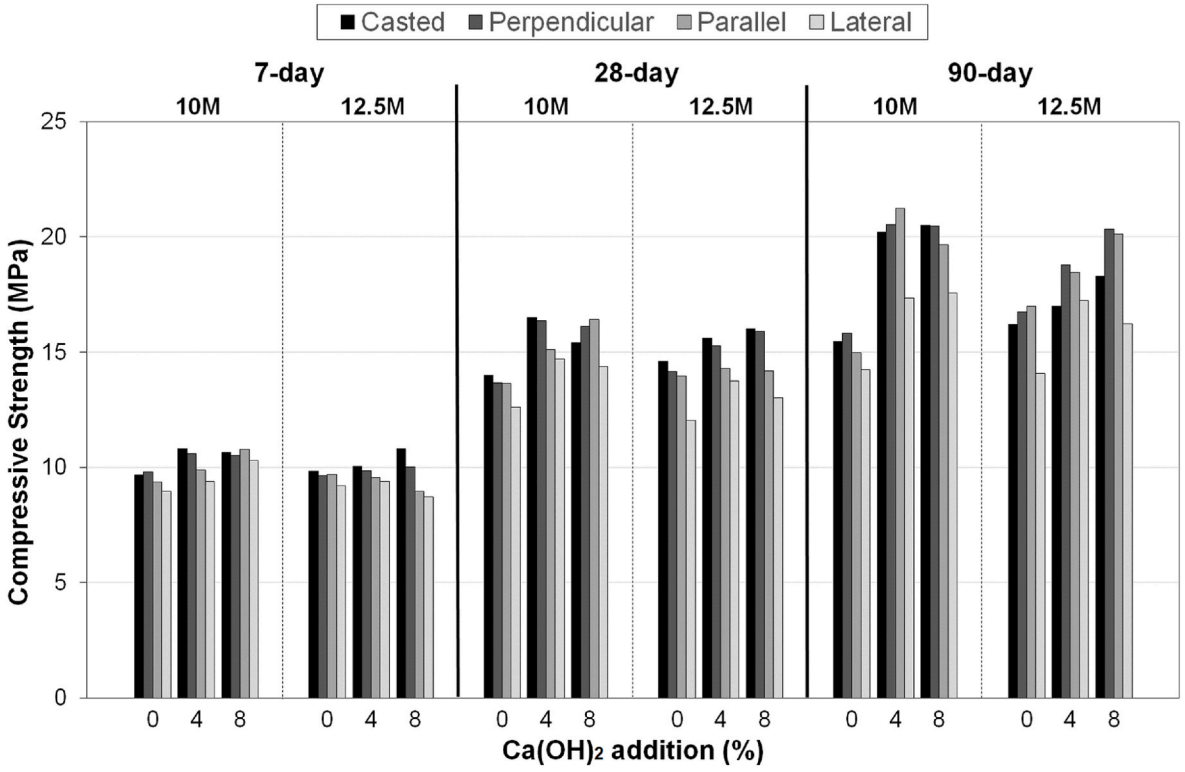

Fig. 6. Average compressive strength results of 3D-printed and mold-casted geopolymer specimens.

mold-casted specimens in different loading directions, regardless of the mixture design; however, the loading direction and alkaline activator content cause differences in the mechanical performance. Therefore, a detailed discussion on how the mechanical performances were affected by the production method (casted and 3D-printed), alkaline activator content, and loading directions is presented in the following sections.

3.1.1. Effect of alkaline activators

When other mixture design parameters were the same, although some variations were observable, an increase in the NaOH molar concentration from 10 to 12.5 M resulted in higher compressive strength results for the mixtures singly activated with NaOH. According to Refs. [35,36], when NaOH molar concentration increases, an increase in the strength of geopolymer mixtures can be expected; however a decrease is also possible. Increase in the NaOH molar concentration increases the alkalinity of the reaction medium and encourages the dissolution of the precursors resulting in an increase in the dissolved Si and Al ions, that can increase the strength of the geopolymers [37–39]. However, higher dissolution rate compared to geopolymerization rate results in the presence of excess dissolved ions in the reaction medium [40–42]. This fact causes (i) restriction in the ion transport because of the repulsive forces between the particles [35,42,43] and (ii) higher silica coagulation and rapid hardening because of the increased Na^+ and $(OH)^-$ ions in the reaction medium [44]. As a result, the increase in the compressive strength results with the increased NaOH concentration can be attributed to higher alkalinity of the geopolymerization medium and thereby

higher dissolution of the precursors.

According to the compressive strength results of both mold-casted and printed specimens given in Fig. 6, common trends were not noted when the $Ca(OH)_2$ utilization rate of the mixtures were increased from 0 to 8% while other parameters were the same. In order to discuss the possible reasons for this, $Ca(OH)_2$-related influencing factors on the compressive strength need to be properly explored and taken into account. In the current literature, there are studies indicating that the mechanical properties of geopolymer mixtures increase with the increase in the utilization rate of $Ca(OH)_2$, and this was attributed to the (i) enhancement in the dissolution of the aluminosilicate precursor with the increased $(OH)^-$ ions in the reaction medium resulting in availability of more active groups to participate in the geopolymerization reactions [45,46], (ii) increase in the precipitation of the C–S–H and C-A-S-H gels and nucleation sites for the formation of geopolymerization products [45,47–51], (iii) ionic charge balancing and seeding effect [49,52–54] and (iv) $CaCO_3$ formation [39,46]. On the other hand, it was also reported that the excessive increase in the utilization rate of $Ca(OH)_2$ decreases the strength of the geopolymer mixtures and the reasons for this were three-fold: (i) lower ionic mobility because of higher ionic concentration [42], (ii) disruption of the optimal gel binder structure because of excess lime content [49], (iii) presence of unreacted lime in the matrix resulting in the creation of the microstructural faults [55]. As can be followed from Fig. 6, there was a general effect of enhancement in the compressive strength of casted and perpendicular-loaded printed specimens with the increased amounts of $Ca(OH)_2$. However, as the utilization rate of $Ca(OH)_2$ increased from 4 to 8%, in mixtures activated by 10M-NaOH, decreases in compressive strength were observed, which can be related to unreacted lime content. Negative effects of $Ca(OH)_2$ at lower molarities can be attributed to the presence of lower amount of reactive dissolved Si and Al species arising from lower dissolution of aluminosilicate materials in the reaction medium with lower alkalinity [35,36]. In addition to the above-mentioned chemical effects, variations in the results can be related to the likely effects of $Ca(OH)_2$ on the fresh properties of the mixtures. As reported in literature [30,31], decrease in the utilization rate of $Ca(OH)_2$ increases the flowability of the geopolymer mortars, and with the increase in flowability it becomes easier to print the fresh mixtures more homogeneously and improve the adhesion between two consecutive printed layers, which can also influence the compressive strength results. In this regard, negative effects of $Ca(OH)_2$ on the compressive strength results generally observed for lateral- and parallel-loaded printed specimens (especially for mixtures activated by 12.5M-NaOH in the case of the increase in the utilization rate of $Ca(OH)_2$ from 4 to 8%) can be associated with the effect of $Ca(OH)_2$ on the fresh properties [63].

3.1.2. Anisotropic behavior and effect of loading direction

Compressive strength results of the mold-casted specimens were lower than specimens loaded perpendicular to the printing directions, irrespective of the curing age (Fig. 6). Many previous studies comparing the compressive strength results of 3D-printed and mold-casted specimens have also reported that 3D-printed specimens could exhibit higher compressive strength than mold-casted specimens [21,56]. This can be explained by the formation of a relatively denser matrix due to the pump pressure during printing. After evaluating the loading direction dependence of the mixtures' compressive strength results, it can be seen that printed specimens loaded in perpendicular direction generally exhibited higher strength results, which is consistent with [25,57], although some natural variations were observed. Higher strength results of the perpendicular-loaded specimens can be attributed to the fact that the loading direction is perpendicular to the bond region. When compressed under perpendicular loading direction, the bond zone between the consecutive printed layers is forced to come together [21]. The load is then transmitted directly through the printed specimen without any negative effect on the bond zone, which can possibly be the reason for the higher performance of the printed specimens under perpendicular loading [58]. This can also be evidenced by the fracture patterns of the different-direction-loaded printed specimens. When a uniform compressive stress is applied to specimens, microcracks start to occur in the matrix at early the stages of loading. With the increments in stress, the cracks begin to propagate throughout the matrix (a growth in diagonal directions). When the stress rises above the critical value, it causes a bridge to form between the cracks formed in the matrix and failure occurs. Therefore, the expected failure shape after the compression test is similar to hourglass [59]. When the failure patterns of the specimens are evaluated (Fig. 7), it was observed that perpendicular-loaded printed specimens had failed like hourglass, meaning that the compressive stress was distributed uniformly throughout the perpendicular-loaded specimens, as in the mold-casted specimens. On the other hand, parallel- and lateral-loaded specimens exhibited a different fracture pattern than the generally expected one under compressive stress. For the loading cases in parallel and lateral directions, after cracks were created by the compressive loading on the specimens reached to the interface bond region, they preferred to propagate along this bonding region resulting in separation of the layers (Fig. 7) [21,58,60]. This type of crack propagation caused relatively brittle failure mode and hence lower compressive strength results for parallel- and lateral-loaded printed specimens were obtained compared to perpendicular-loaded ones. Considering all these statements, it can be stated that the path of propagation chosen by the microcracks has a significant role on the mechanical properties of the printed specimens. Well compaction of the fresh mixtures in the perpendicular direction owing to the self-weight of the extruded layers can be another possible contributor of better compressive strength results under loading in perpendicular direction. Compressive strength results of parallel-loaded specimens were higher than those of lateral-loaded specimens, which can be attributed to the increased intensity of the fresh mixture in parallel to the nozzle movement direction due to considerable pumping pressure on the 3D-printed layer over the extrusion process [21,27,61–63].

According to TBEC 2018 [64], the mortar compressive strength of masonry walls varies between 1.4 and 14.6 MPa, depending on the mortar class. According to IBC 2015, the compressive strength of the masonry must be 2.07 MPa on average and at least 1.7 MPa. The compressive strengths of masonry structures determined in MSJC and based on the work of Noland and Kingsley [65] should be between 10.34 and 27.58 MPa. In accordance with the compressive strength results obtained herein, the compressive strength of the entirely CDW-based geopolymer mortars met the values reported by all three standards for the construction of masonry walls.

3.2. Flexural strength

Flexural strength of 3D-printed CDW-based geopolymer mortar specimens were tested for the loading in the directions perpendicular and lateral to the printing path to evaluate performance differences between mold-casted and layered specimens, anisotropic behavior of the 3D-printed specimens, and effects of alkaline activator content on the flexural performance of the mixtures. 7-, 28- and 90-day average flexural strength results of both mold-casted and 3D-printed specimens subjected to ambient curing conditions are shown in Fig. 8. Flexural strength of the mixtures increased continuously with the extended curing ages because of the ongoing geopolymerization reactions [66]. Maximum flexural strength results for mold-casted, perpendicular-loaded and lateral-loaded 3D-printed specimens were recorded from the mixture activated by 10 M NaOH and 4% $Ca(OH)_2$. The average flexural strength reached the maximum values of 4.9 MPa, 6.6 MPa, and 4.7 MPa for the mold-casted specimens, perpendicular-loaded and lateral-loaded 3D-printed specimens after 90 days, respectively. Obtained flexural strength results of perpendicular-loaded and lateral-loaded 3D-printed specimens were compatible with several research results [23,26,27,57,67–71]. Results demonstrated that

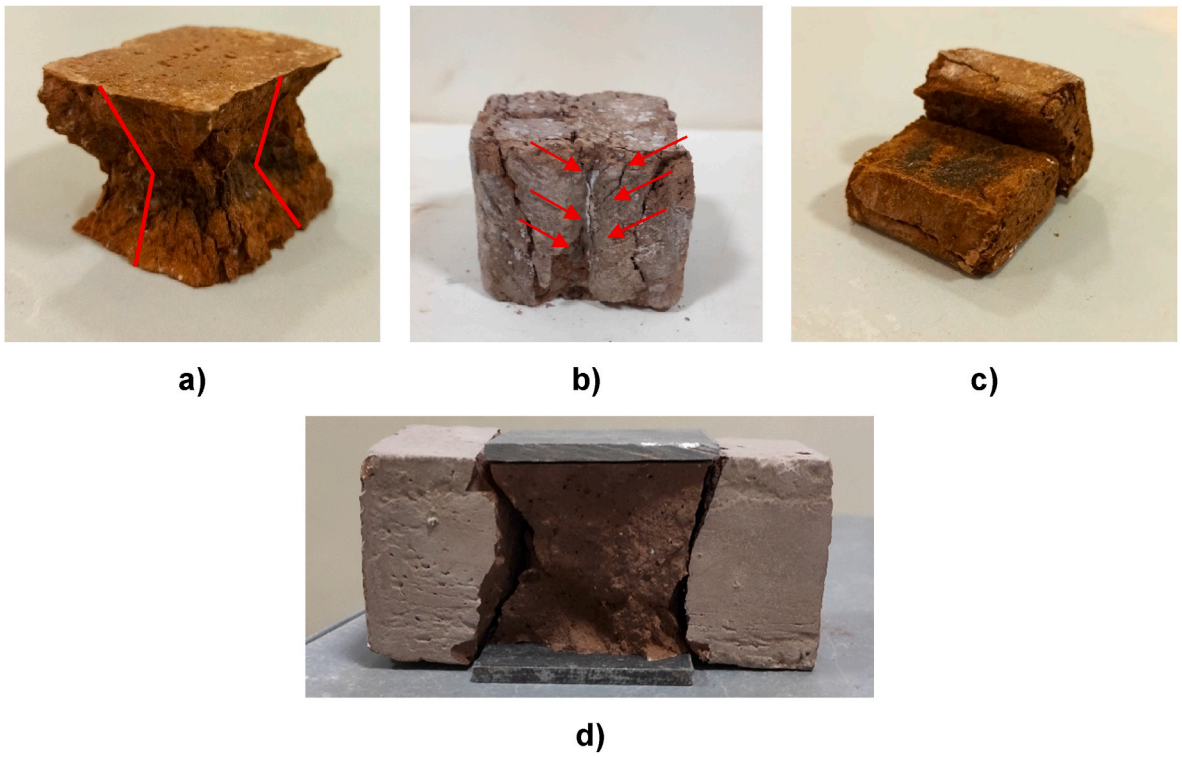

Fig. 7. Representative images showing details of failure mode of compression specimens in a) perpendicular, b) parallel, c) lateral direction, d) casted specimen.

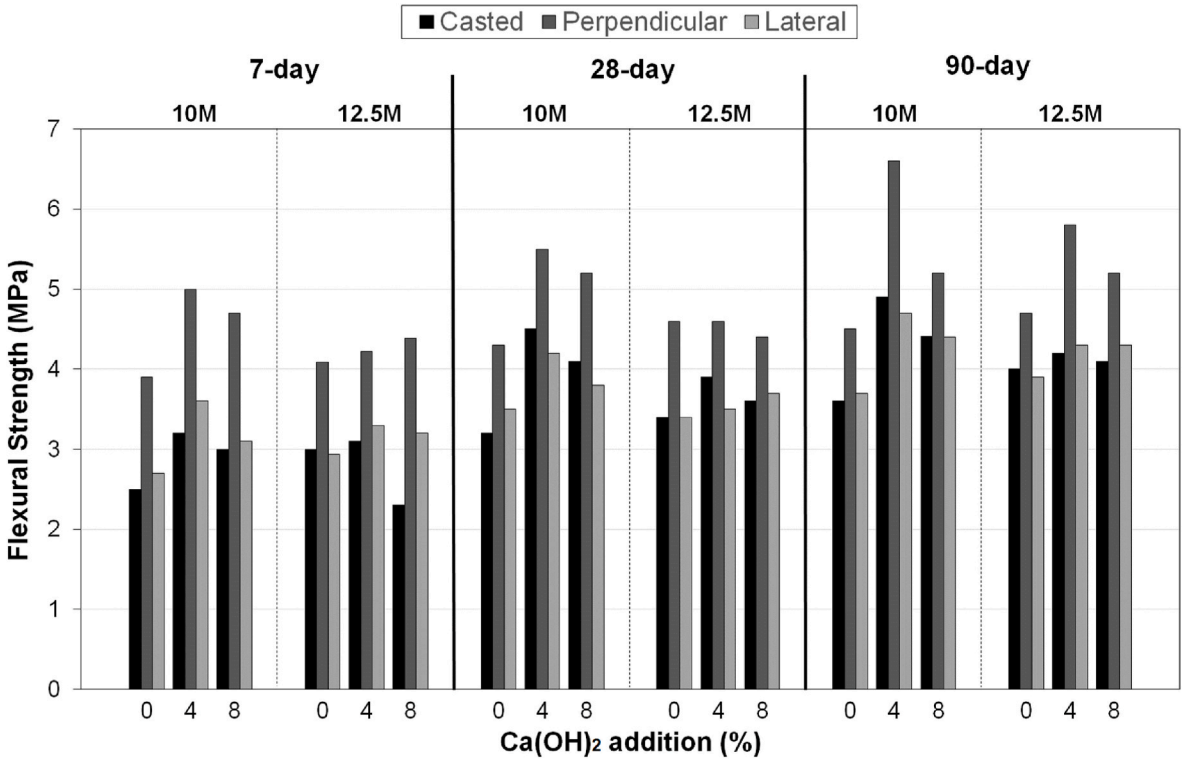

Fig. 8. Average flexural strength results of 3D-printed and mold-casted geopolymer specimens.

flexural strength of 3D-printed specimens loaded in perpendicular direction were higher than those of both mold-casted and lateral-loaded 3D-printed specimens. In general, mold-casted and lateral-loaded 3D-printed specimens showed similar performances for all testing ages with slight deviations.

3.2.1. *Effect of alkaline activators*

Flexural strength results of the mold-casted specimens activated solely with 10 M NaOH were lower than those of mold-casted specimens activated with 12.5 M NaOH. Similar results were also obtained from the 3D-printed geopolymer mixtures activated solely with NaOH. Increment

of NaOH molarity, therefore, was favorable for the flexural strength performance of CDW-based geopolymer mortar mixtures activated solely with NaOH. The possible reasons for the positive effects of increased NaOH molarity on the strength development were discussed in the previous section and are also valid for flexural strength results.

Inclusion of $Ca(OH)_2$ into mixtures activated singly with NaOH yielded increments in flexural strength results of both casted and 3D-printed specimens, since the increment of Ca sources in the medium may lead to the formation of more strength-giving geopolymer products (*e.g.*, C-(A)-S-H, N-A-S-H) in the matrix and effective bond area [45,47–51]. However, addition of 8% $Ca(OH)_2$ either decreased or did not make a positive contribution to the flexural strength results, irrespective of NaOH molarity. The possible effects of 8% $Ca(OH)_2$ addition could be due to lower ionic mobility, disruption of gel structure, presence of unreacted lime [42,49,55]. In addition, for the 3D-printed specimens, increment of $Ca(OH)_2$ content in the matrix may lead to weaknesses in the effective bond area because of the redundant increment in viscosity (Table 2).

The trend observed for the compressive strength results of casted and perpendicular-loaded 3D-printed specimens activated with 12.5 M NaOH – 8% $Ca(OH)_2$ did not coincide with the flexural strength results of the same mixtures. This can possibly be attributed to the variations in the fracture mechanism and load distribution on the specimens and test methods since the compressive strength results of lateral- and parallel-loaded 3D-printed specimens coincided with the flexural strength test results of both mold-casted and 3D-printed specimens. For the flexural strength, applied load was directly delivered to the effective bond area that made the bond area more essential than the matrix. Although increments in the $Ca(OH)_2$ content may lead to more geopolymerization products in the matrix, due to more viscous structure, more voids can form in the effective bond area which may lead to reductions in flexural strength with the increment of $Ca(OH)_2$ from 4 to 8% in the mixtures activated with 12.5 M NaOH. It seems that the enhancements in the geopolymer matrix favoring the flexural strength could not overcome the negative effects of high viscosity resulting in weaknesses in the bonding zone [63] (Fig. 11).

3.2.2. Direction-dependence of mechanical properties

In addition to the effects of alkaline activators, anisotropic behavior of the mixtures was evaluated by considering the flexural performance of 3D-printed specimens. According to the obtained test results, flexural strength of the mold-casted specimens was similar to or lower than that of 3D-printed specimens for each testing age. The possible reason for the improved flexural strength performance of 3D-printed specimens (although decrement was expected because of layer-by-layer production) can be better compaction of the mixtures due to high-pressure pump, considering the fact that the amount of air voids is significantly effective on the flexural strength [56]. Increased air void formation was observed in geopolymer specimens during casting in comparison with the 3D-printed counterparts, as the developed CDW-based geopolymers have sticky nature due to clayey nature [30,31].

During printing, because of both the weight of the upper layer and pushing of pressurized consecutive materials by the pump, better compaction was achieved in the bottom layer of prismatic specimens. Production-related parameters are significantly effective on the performance of the mixtures. Moreover, load distribution pattern of 3D-printed specimen was also effective on the performance of CDW-based geopolymer mortar mixtures. According to the obtained results, perpendicular-loaded 3D-printed specimens had higher flexural strength than that of lateral-loaded ones for each mixture and testing age. Considering that during the flexural strength testing in perpendicular direction, first layer, which was more compacted and bonded, was in the tension zone, it yielded better performance. Moreover, 3D-printed specimens loaded in the lateral direction tended to separate from the weak bond area between the two consecutive printed layers, causing them to fail quickly under flexure. When the fracture behaviors are examined, the fracture behavior presented in Fig. 9a is close to parallel to the perpendicular reference line. However, when Fig. 9b is examined, the fracture behavior is parallel to the reference line until it reaches the bond area, deviating thereafter. The weakness in this area may cause deviation in the cracking path and the flexural strength to decrease by up to 29% considering the printing direction.

3.3. Splitting and direct tensile strength (bond strength)

7-, 28- and 90-day splitting and direct tensile test results of the printed specimens cured under ambient conditions are represented in Fig. 10. As seen from the figure, tensile strength results obtained from both splitting and direct test methods were generally consistent with each other. The tensile strength result of the mixtures increased continuously with the extended curing ages as a result of ongoing geopolymerization reactions. Maximum splitting and direct tensile strength results for each curing age were recorded from the geopolymer mixture activated with 10 M NaOH – 4% $Ca(OH)_2$, where the splitting and direct tensile strength results reached the maximum values of 1.35 and 1.79 MPa after 90-day ambient curing, respectively.

On contrary to the compressive and flexural strength results, increments in the NaOH molarity did not lead to increments in the splitting and direct tensile strength test results. On one hand, increment in NaOH molarity may increase the dissolution of precursors resulting in increases in the production of geopolymerization products, while on the other hand, the viscosity of the mixtures may increase, leading to the formation of voids in the matrix and weak bonding capacity (weak effective bond area) between the consecutive printed layers [30,31,63]. According to the obtained results, the bond strength of the geopolymer mixtures increased with the usage of $Ca(OH)_2$ up to 4%, irrespective of the NaOH molarity. Increment in the bond strength could be attributed to the formation of more geopolymerization products on effective bond area and matrix (Fig. 11a), and improved interfacial tranisiton zone between the geopolymer paste and aggregates due to lower porosity in the presence of high calcium content [72–74]. The relatively low tensile strength results of geopolymer mixtures activated with 10 M and 12.5 M NaOH containing more than 4% $Ca(OH)_2$ can be explained by the fact that, unreacted excessive alkaline activator content disrupts the homogeneity of the mixture and, decreased workability with the increased $Ca(OH)_2$ content may lead to weak bonding between the layers as the voids formed prevent the synthesis of strength-giving products between the layers (Fig. 11b). The tensile strength results of CDW-based geopolymer mortars here were comparable with those reported in literature [70,75–77].

Our results showed that mechanical properties of 3D-printed entirely CDW-based geopolymer mortars are driven by the rheology of the mixtures and geopolymerization reactions simultaneously. Improvements in the matrix due to alkaline content were more influential for the mechanical performance of the mold-casted and perpendicular-loaded printed specimens due to less stress formation in the bond area. However, viscosity properties had more dominant effects on the mechanical properties of the parallel- and lateral-loaded specimens since the applied load concentrated in the bond area, and adhesion between the layers was mainly affected by the fresh properties. It was shown that the bond performance between the layers is one of the main reasons for the anisotropic behavior of 3D-printed structures. Furthermore, bond strength evaluation showed that although the matrix was enhanced with the alkaline content optimization, due to higher viscosity resulting in poor adhesion between the layers, lower bond strength performance was recorded from geopolymer mortars. Thereofore, in order to eliminate the anisotropic performance of printed structures, bond adhesion between the layers should be taken into account considering viscosity along with the matrix performance while designing the mixtures. With the improved bond adhesion, therefore it will be possible to diminish directional performance variations for the geopolymer systems based on CDW entirely.

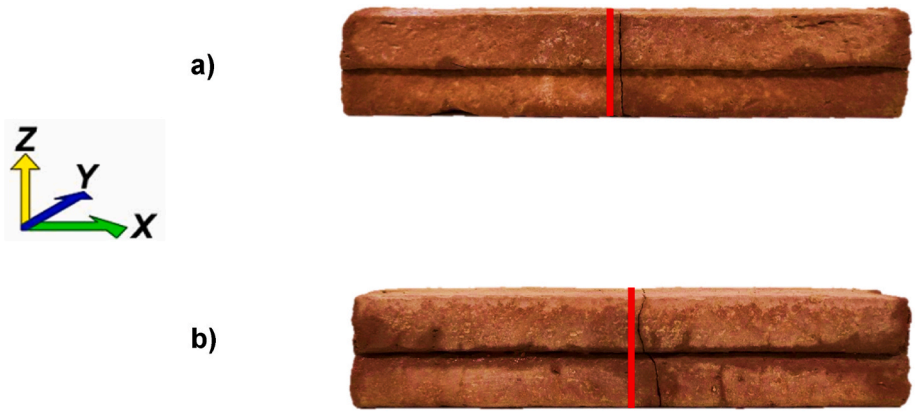

Fig. 9. Representative images showing the failure modes of flexural test specimen in a) perpendicular (loaded in z axis) b) lateral (loaded in y axis) direction.

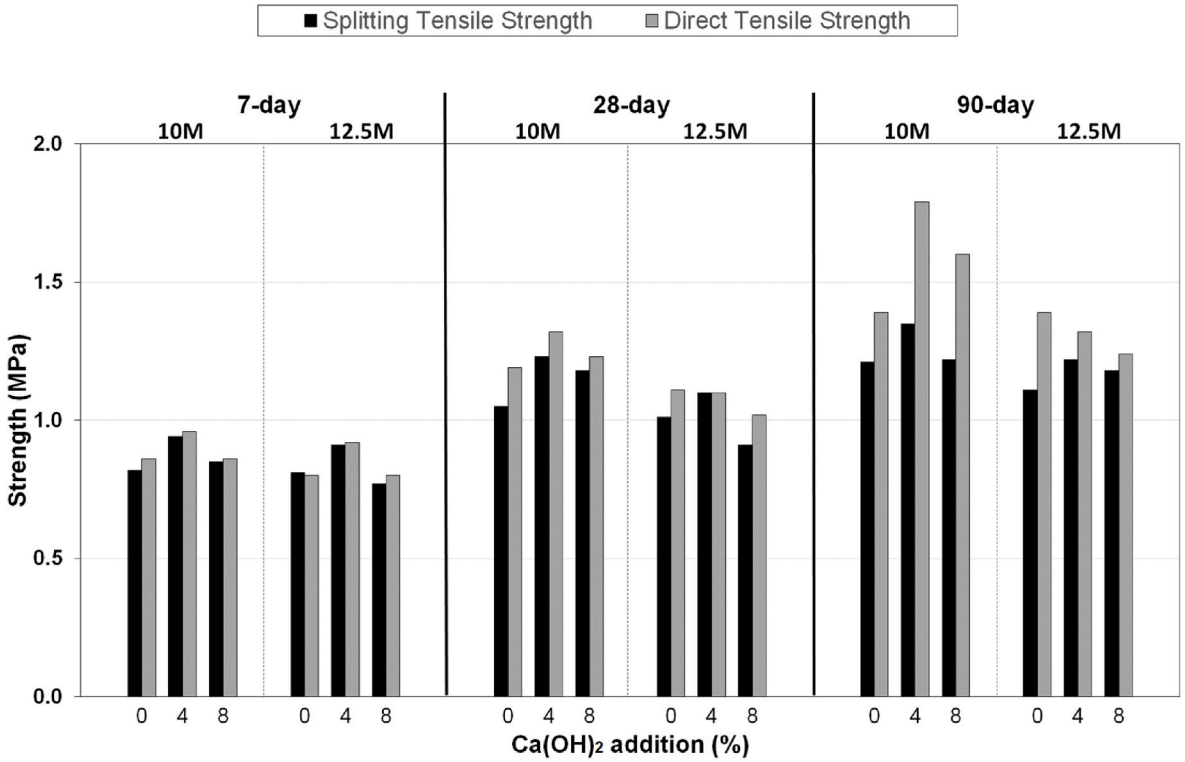

Fig. 10. Average splitting and direct tensile strength results of 3D-printed geopolymer specimens.

4. Conclusions

This study aimed at evaluating direction-dependent performance of 3D-printed entirely CDW-based geopolymer mortars. The study also focused on determining the effect of alkaline activators on the mechanical properties of 3D-printed geopolymer mortars such as compressive, flexural and bond strengths. 3D-printed and mold-casted specimens' performances were compared with each other to examine production method-related variations in the mechanical properties of the geopolymer mortars. The mixtures were activated with 10 M and 12.5 M NaOH and 0%, 4% and 8% (by the total weight of precursors) $Ca(OH)_2$ in various combinations, and specimens were cured under ambient conditions. The following results were drawn:

- For the mixtures activated by the single use of NaOH, increasing the NaOH molarity from 10 to 12.5 M increased the compressive and flexural strengths of the mold-casted and 3D-printed specimens, irrespective of the curing age. However, with the increased NaOH molarity, splitting and direct tensile strength results of the 3D-printed specimens decreased most probably due to the increase in the viscosity of the mixtures leading to lower adhesion in the interfacial bonding region between the layers.
- Mechanical properties of the CDW-based geopolymer mortars increased with inclusion of $Ca(OH)_2$ at utilization rate of 4%. However, beyond this rate, enhancement effects of $Ca(OH)_2$ utilization on mechanical properties (except compressive strength) were not observed, most probably due to the excessive increase in the viscosity of mixtures suppressing the positive effects of $Ca(OH)_2$ in geopolymerization.
- Direction-dependent tests performed on 3D-printed mortar specimens indicated that printed CDW-based specimens have anisotropic feature. In terms of direction-dependent compressive strength results, in general, among mold-casted and three different loading directions including perpendicular, parallel and lateral to the printing

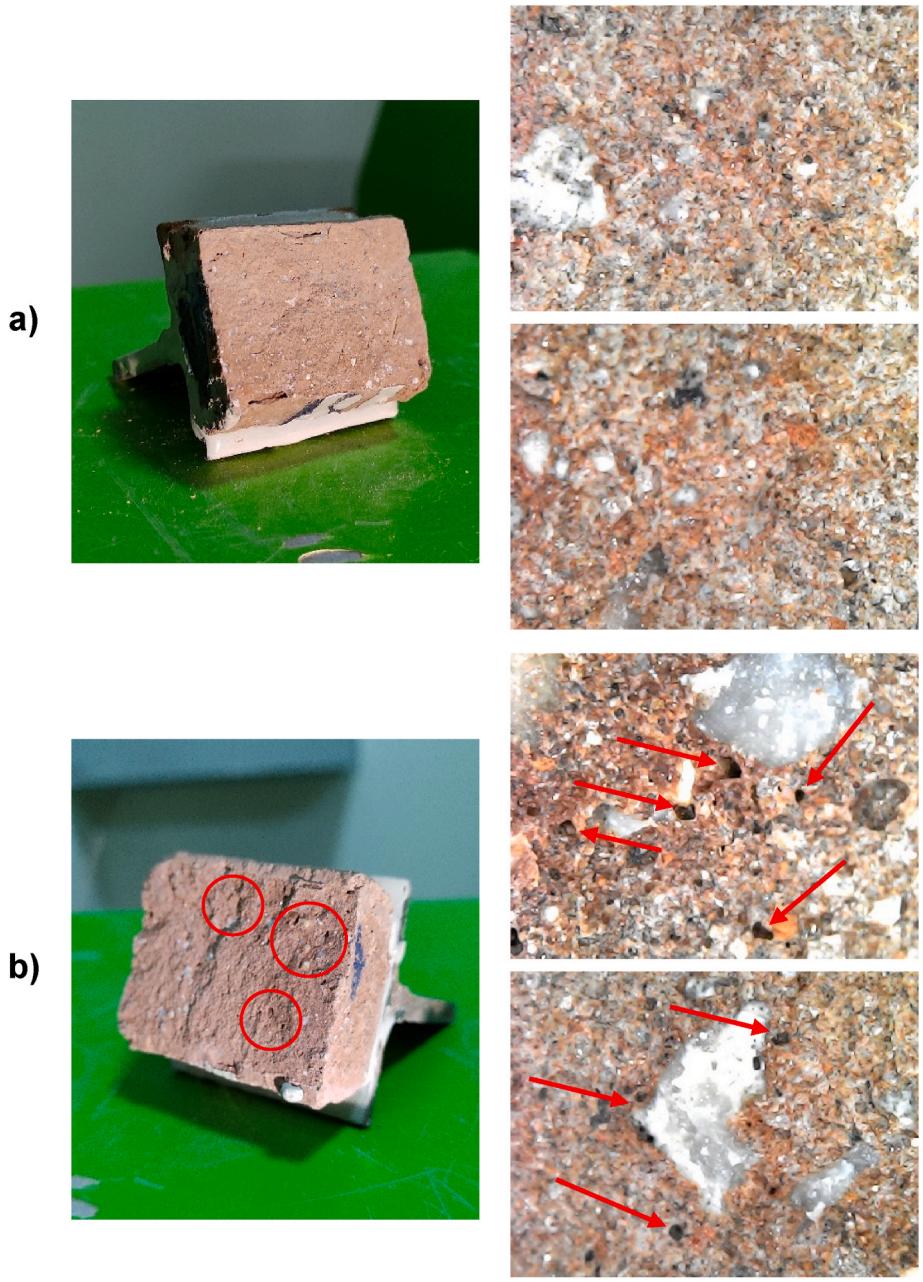

Fig. 11. Representative general and close-up views of (area of 3.2 × 2.4 mm^2) a) non-porous and, b) porous bond zone.

path, irrespective of the curing age, the compressive strength results were the highest for perpendicular loading direction with the decreasing order for mold-casted, parallel direction and lateral direction.

- In terms of direction-dependent flexural strength results, between two different loading directions including perpendicular and lateral to printing direction, irrespective of the curing age, specimens loaded in perpendicular to the printing direction exhibited better performance compared to those loaded in lateral to the printing direction. As in the compressive strength tests, perpendicular-loaded specimens exhibited higher flexural strength performance than mold-casted ones. In addition, lateral-loaded and mold-casted specimens showed similar flexural performances.
- At the end of 90-day ambient curing, compressive strength results recorded for the mold-casted and 3D-printed entirely CDW-based specimens reached approximately 20 MPa and met the values of relevant standards for construction of masonry walls.
- Geopolymer mortars showed anisotropic properties in compressive and flexural strength tests. In compressive strength results of the 3D-printed specimens loaded in different directions, the maximum direction dependent variation reached to the level of 20%, while this level was 30% for flexural strength results. The anisotropic behavior of the 3D-printed geopolymer mortar specimens is considered to be a natural feature of the layer-by-layer printing process.

Declaration of competing interest

The authors declare that they have no known competing financial interests or personal relationships that could have appeared to influence the work reported in this paper.

Data availability

No data was used for the research described in the article.

Acknowledgement

The authors gratefully acknowledge the financial assistance of the Scientific and Technical Research Council (TUBITAK) of Turkey provided under Project: 119M630 and 119N030.

References

[1] T. Bock, The future of construction automation: technological disruption and the upcoming ubiquity of robotics, Autom. ConStruct. 59 (2015), https://doi.org/10.1016/j.autcon.2015.07.022.
[2] R. Maskuriy, A. Selamat, P. Maresova, O. Krejcar, O. David, Industry 4.0 for the construction industry: review of management perspective, Economies 7 (2019) 14, https://doi.org/10.3390/economies7030068.
[3] F. Bos, R. Wolfs, Z. Ahmed, T. Salet, Additive manufacturing of concrete in construction: potentials and challenges of 3D concrete printing, Virtual Phys. Prototyp. 11 (3) (2016) 209–225, https://doi.org/10.1080/17452759.2016.1209867.
[4] E. Lloret, A.R. Shahab, M. Linus, R.J. Flatt, F. Gramazio, M. Kohler, S. Langenberg, Complex concrete structures: merging existing casting techniques with digital fabrication, Comput. Aided Des. 60 (2015) 40–49, https://doi.org/10.1016/j.cad.2014.02.011.
[5] P. Shakor, J. Sanjayan, A. Nazari, S. Nejadi, Modified 3D printed powder to cement-based material and mechanical properties of cement scaffold used in 3D printing, Construct. Build. Mater. 138 (2017) 398–409, https://doi.org/10.1016/j.conbuildmat.2017.02.037.
[6] M. Mohammad, E. Masad, S.G. Al-Ghamdi, 3D concrete printing sustainability: a comparative life cycle assessment of four construction method scenarios, Buildings 10 (12) (2020) 245, https://doi.org/10.3390/buildings10120245.
[7] J. Biernacki, J. Bullard, G. Sant, K. Brown, F. Glasser, S. Jones, M. Ley, R. Livingston, L. Nicoleau, J. Olek, F. Sanchez, R. Shahsavari, P. Stutzman, K. Sobolev, T. Prater, Cements in the 21 st century: challenges, perspectives, and opportunities, J. Am. Ceram. Soc. 100 (2017), https://doi.org/10.1111/jace.14948.
[8] S. Keating, N.A. Spielberg, J. Klein, N. Oxman, A Compound Arm Approach to Digital Construction, Robotic Fabrication in Architecture, Art and Design, 2014, pp. 99–110, https://doi.org/10.1007/978-3-319-04663-1_7. Springer2014.
[9] G. Beersaerts, S.S. Lucas, Y. Pontikes, An Fe-Rich Slag-Based Mortar for 3D Printing, RILEM International Conference on Concrete and Digital Fabrication, Springer, 2020, pp. 3–12, https://doi.org/10.1007/978-3-030-49916-7_1.
[10] Z. Peng, W. Lu, C.J. Webster, Quantifying the embodied carbon saving potential of recycling construction and demolition waste in the Greater Bay Area, China: status quo and future scenarios, Sci. Total Environ. 792 (2021), 148427, https://doi.org/10.1016/j.scitotenv.2021.148427.
[11] M.M. Sabai, M.G.D.M. Cox, R.R. Mato, E.L.C. Egmond, J.J.N. Lichtenberg, Concrete block production from construction and demolition waste in Tanzania, Resour. Conserv. Recycl. 72 (2013) 9–19, https://doi.org/10.1016/j.resconrec.2012.12.003.
[12] Mineral Commodity Summaries 2019, Mineral Commodity Summaries, Reston, VA, 2019, https://doi.org/10.3133/70202434.
[13] M. Taylor, C. Tam, D. Gielen, Energy efficiency and CO2 emissions from the, Global Cement Industry (2006) 50.
[14] US EPA, Advancing Sustainable Materials Management: 2017, United States Environmental Protection Agency, 2019.
[15] European Commision, Directorate-General for Environment, Resource Efficient Use of Mixed Wastes Improving Management of Construction and Demolition Waste : Final Report, Publications Office, 2017, https://doi.org/10.2779/99903.
[16] M. Bravo, J. de Brito, J. Pontes, L. Evangelista, Mechanical performance of concrete made with aggregates from construction and demolition waste recycling plants, J. Clean. Prod. 99 (2015) 59–74, https://doi.org/10.1016/j.jclepro.2015.03.012.
[17] A. Arulrajah, M. Ali, M.M. Disfani, J. Piratheepan, M. Bo, Geotechnical performance of recycled glass-waste rock blends in footpath bases, J. Mater. Civ. Eng. 25 (5) (2013) 653–661, https://doi.org/10.1061/(ASCE)MT.1943-5533.0000617.
[18] M. Contreras, S.R. Teixeira, M.C. Lucas, L.C.N. Lima, D.S.L. Cardoso, G.A.C. da Silva, G.C. Gregório, A.E. de Souza, A. dos Santos, Recycling of construction and demolition waste for producing new construction material (Brazil case-study), Construct. Build. Mater. 123 (2016) 594–600, https://doi.org/10.1016/j.conbuildmat.2016.07.044.
[19] A. Arulrajah, M. Ali, M.M. Disfani, S. Horpibulsuk, Recycled-glass blends in pavement base/subbase applications: laboratory and field evaluation, J. Mater. Civ. Eng. 26 (7) (2014), 04014025, https://doi.org/10.1061/(ASCE)MT.1943-5533.0000966.
[20] M. Chougan, S.H. Ghaffar, M. Jahanzat, A. Albar, N. Mujaddedi, R. Swash, The influence of nano-additives in strengthening mechanical performance of 3D printed multi-binder geopolymer composites, Construct. Build. Mater. 250 (2020), 118928, https://doi.org/10.1016/j.conbuildmat.2020.118928.
[21] B. Panda, S.C. Paul, L.J. Hui, Y.W.D. Tay, M.J. Tan, Additive manufacturing of geopolymer for sustainable built environment, J. Clean. Prod. 167 (2017) 281–288, https://doi.org/10.1016/j.jclepro.2017.08.165.
[22] B. Nematollahi, P. Vijay, J. Sanjayan, A. Nazari, M. Xia, V.N. Nerella, V. Mechtcherine, Effect of polypropylene fibre addition on properties of geopolymers made by 3D printing for digital construction, Materials 11 (2018) 2352, https://doi.org/10.3390/ma11122352.
[23] S.H. Bong, M. Xia, B. Nematollahi, C. Shi, Ambient temperature cured 'just-add-water' geopolymer for 3D concrete printing applications, Cement Concr. Compos. 121 (2021), 104060, https://doi.org/10.1016/j.cemconcomp.2021.104060.
[24] B. Panda, C. Unluer, M.J. Tan, Investigation of the rheology and strength of geopolymer mixtures for extrusion-based 3D printing, Cement Concr. Compos. 94 (2018) 307–314, https://doi.org/10.1016/j.cemconcomp.2018.10.002.
[25] B. Panda, S. Chandra Paul, M. Jen Tan, Anisotropic mechanical performance of 3D printed fiber reinforced sustainable construction material, Mater. Lett. 209 (2017) 146–149, https://doi.org/10.1016/j.matlet.2017.07.123.
[26] B. Nematollahi, M. Xia, P. Vijay, J.G. Sanjayan, Properties of Extrusion-Based 3D Printable Geopolymers for Digital Construction Applications, 3D Concrete Printing Technology, Elsevier2019, pp. 371-388. https://doi.org/10.1016/B978-0-12-815481-6.00018-X. .
[27] B. Nematollahi, M. Xia, S.H. Bong, J. Sanjayan, Hardened Properties of 3D Printable 'one-Part' geopolymer for Construction Applications, RILEM International Conference on Concrete and Digital Fabrication, Springer, 2018, pp. 190–199, https://doi.org/10.1007/978-3-319-99519-9_17.
[28] S. Muthukrishnan, S. Ramakrishnan, J. Sanjayan, Effect of alkali reactions on the rheology of one-part 3D printable geopolymer concrete, Cement Concr. Compos. 116 (2020), 103899, https://doi.org/10.1016/j.cemconcomp.2020.103899.
[29] A. Bouaissi, L.Y. Li, L.M. Moga, I.G. Sandu, M. Abdullah, A.V. Sandu, A review on fly ash as a raw cementitious material for geopolymer concrete, Rev. Chim 69 (7) (2018) 1661–1667, https://doi.org/10.37358/rc.18.7.6390.
[30] H. Ilcan, O. Sahin, A. Kul, G. Yildirim, M. Sahmaran, Rheological properties and compressive strength of construction and demolition waste-based geopolymer mortars for 3D-Printing, Construct. Build. Mater. 328 (2022), 127114, https://doi.org/10.1016/j.conbuildmat.2022.127114.
[31] O. Şahin, H. İlcan, A.T. Ateşli, A. Kul, G. Yıldırım, M. Şahmaran, Construction and demolition waste-based geopolymers suited for use in 3-dimensional additive manufacturing, Cement Concr. Compos. 121 (2021), 104088, https://doi.org/10.1016/j.cemconcomp.2021.104088.
[32] ASTM C496/496M-17, Standard Test Method for Splitting Tensile Strength of Cylindrical Concrete Specimens, ASTM International, 2017, https://doi.org/10.1520/C0496-96.
[33] S. Timoshenko, J.N. Goodier, Theory of Elasticity, McGraw-Hill Book Company, London, 1970.
[34] A.U. Rehman, J.-H. Kim, 3D concrete printing: a systematic review of rheology, mix designs, mechanical, microstructural, and durability characteristics, Materials 14 (14) (2021) 3800, https://doi.org/10.3390/ma14143800.
[35] D. Khale, R. Chaudhary, Mechanism of geopolymerization and factors influencing its development: a review, J. Mater. Sci. 42 (3) (2007) 729–746, https://doi.org/10.1007/s10853-006-0401-4.
[36] S.V. Patankar, Y.M. Ghugal, S.S. Jamkar, Effect of concentration of sodium hydroxide and degree of heat curing on fly ash-based geopolymer mortar, Indian journal of materials science 2014 (2014), https://doi.org/10.1155/2014/938789.
[37] U. Rattanasak, P. Chindaprasirt, Influence of NaOH solution on the synthesis of fly ash geopolymer, Miner. Eng. 22 (12) (2009) 1073–1078, https://doi.org/10.1016/j.mineng.2009.03.022.
[38] M. Komljenović, Z. Baščarević, V. Bradić, Mechanical and microstructural properties of alkali-activated fly ash geopolymers, J. Hazard Mater. 181 (1–3) (2010) 35–42, https://doi.org/10.1016/j.jhazmat.2010.04.064.
[39] H.Y. Leong, D.E.L. Ong, J.G. Sanjayan, A. Nazari, The effect of different Na2O and K2O ratios of alkali activator on compressive strength of fly ash based-geopolymer, Construct. Build. Mater. 106 (2016) 500–511, https://doi.org/10.1016/j.conbuildmat.2015.12.141.
[40] R.M. Hamidi, Z. Man, K.A. Azizli, Concentration of NaOH and the effect on the properties of fly ash based geopolymer, Procedia Eng. 148 (2016) 189–193, https://doi.org/10.1016/j.proeng.2016.06.568.
[41] A.B. Pascual, M.T. Tognonvi, A. Tagnit-Hamou, Waste glass powder-based alkali-activated mortar, Int. J. Res. Eng. Technol 3 (13) (2014) 32–36.
[42] S. Alonso, A. Palomo, Alkaline activation of metakaolin and calcium hydroxide mixtures: influence of temperature, activator concentration and solids ratio, Mater. Lett. 47 (1–2) (2001) 55–62, https://doi.org/10.1016/S0167-577X(00)00212-3.
[43] Y. Rifaai, A. Yahia, A. Mostafa, S. Aggoun, E.-H. Kadri, Rheology of fly ash-based geopolymer: effect of NaOH concentration, Construct. Build. Mater. 223 (2019) 583–594, https://doi.org/10.1016/j.conbuildmat.2019.07.028.
[44] A. Palomo, M. Grutzeck, M. Blanco, Alkali-activated fly ashes: a cement for the future, Cement Concr. Res. 29 (8) (1999) 1323–1329, https://doi.org/10.1016/S0008-8846(98)00243-9.
[45] M.L. Granizo, S. Alonso, M.T. Blanco-Varela, A. Palomo, Alkaline activation of metakaolin: effect of calcium hydroxide in the products of reaction, J. Am. Ceram. Soc. 85 (1) (2002) 225–231, https://doi.org/10.1111/j.1151-2916.2002.tb00070.x.
[46] B. Akturk, A.B. Kizilkanat, N. Kabay, Effect of calcium hydroxide on fresh state behavior of sodium carbonate activated blast furnace slag pastes, Construct. Build. Mater. 212 (2019) 388–399, https://doi.org/10.1016/j.conbuildmat.2019.03.328.
[47] X. Chen, A. Sutrisno, L.J. Struble, Effects of calcium on setting mechanism of metakaolin-based geopolymer, J. Am. Ceram. Soc. 101 (2) (2018) 957–968, https://doi.org/10.1111/jace.15249.
[48] X. Guo, H. Shi, L. Chen, W.A. Dick, Alkali-activated complex binders from class C fly ash and Ca-containing admixtures, J. Hazard Mater. 173 (1–3) (2010) 480–486, https://doi.org/10.1016/j.jhazmat.2009.08.110.
[49] H. Khater, Effect of calcium on geopolymerization of aluminosilicate wastes, J. Mater. Civ. Eng. 24 (1) (2012) 92–101, https://doi.org/10.1061/(ASCE)MT.1943-5533.0000352.

[50] J. Temuujin, A. van Riessen, R. Williams, Influence of calcium compounds on the mechanical properties of fly ash geopolymer pastes, J. Hazard Mater. 167 (1) (2009) 82–88, https://doi.org/10.1016/j.jhazmat.2008.12.121.
[51] C.K. Yip, G. Lukey, J.S. Van Deventer, The coexistence of geopolymeric gel and calcium silicate hydrate at the early stage of alkaline activation, Cement Concr. Res. 35 (9) (2005) 1688–1697, https://doi.org/10.1016/j.cemconres.2004.10.042.
[52] J. Davidovits, Geopolymers: inorganic polymeric new materials, J. Therm. Anal. Calorim. 37 (8) (1991) 1633–1656, https://doi.org/10.1007/bf01912193.
[53] X. Guo, H. Shi, Metakaolin-, fly ash-and calcium hydroxide-based geopolymers: effects of calcium on performance, Adv. Cement Res. 27 (10) (2015) 559–566, https://doi.org/10.1680/jadcr.14.00081.
[54] C. Li, H. Sun, L. Li, A review: the comparison between alkali-activated slag (Si+ Ca) and metakaolin (Si+ Al) cements, Cement Concr. Res. 40 (9) (2010) 1341–1349, https://doi.org/10.1016/j.cemconres.2010.03.020.
[55] J. Gourley, Geopolymers; Opportunities for Environmentally Friendly Construction Materials, Materials 2003 Conference: Adaptive Materials for a Modern Society, Institute of Materials Engineering Australia, Sydney, 2003.
[56] T.T. Le, S.A. Austin, S. Lim, R.A. Buswell, R. Law, A.G.F. Gibb, T. Thorpe, Hardened properties of high-performance printing concrete, Cement Concr. Res. 42 (3) (2012) 558–566, https://doi.org/10.1016/j.cemconres.2011.12.003.
[57] S. Muthukrishnan, S. Ramakrishnan, J. Sanjayan, Effect of alkali reactions on the rheology of one-part 3D printable geopolymer concrete, Cement Concr. Compos. 116 (2021), 103899, https://doi.org/10.1016/j.cemconcomp.2020.103899.
[58] K. Yu, W. McGee, T.Y. Ng, H. Zhu, V.C. Li, 3D-printable engineered cementitious composites (3DP-ECC): fresh and hardened properties, Cement Concr. Res. 143 (2021), 106388, https://doi.org/10.1016/j.cemconres.2021.106388.
[59] P.K. Mehta, Concrete : Microstructure, Properties, and Materials, McGraw-Hill, New York, 2006.
[60] M. Moini, Buildability and Mechanical Performance of Architectured Cement-Based Materials Fabricated Using a Direct-Ink-Writing Process, Purdue University Graduate School, 2020.
[61] J.H. Lim, B. Panda, Q.-C. Pham, Improving flexural characteristics of 3D printed geopolymer composites with in-process steel cable reinforcement, Construct. Build. Mater. 178 (2018) 32–41, https://doi.org/10.1016/j.conbuildmat.2018.05.010.
[62] B. Panda, G.V.P.B. Singh, C. Unluer, M.J. Tan, Synthesis and characterization of one-part geopolymers for extrusion based 3D concrete printing, J. Clean. Prod. 220 (2019) 610–619, https://doi.org/10.1016/j.jclepro.2019.02.185.
[63] J.G. Sanjayan, B. Nematollahi, M. Xia, T. Marchment, Effect of surface moisture on inter-layer strength of 3D printed concrete, Construct. Build. Mater. 172 (2018) 468–475, https://doi.org/10.1016/j.conbuildmat.2018.03.232.
[64] TBEC, Turkish Seismic Earthquake Code, 2018, pp. 1–146.
[65] J.L. Noland, U.S. Coordinated program for masonry building research, in: L. S. Beedle (Ed.), Second Century of the Skyscraper: Council on Tall Buildings and Urban Habitat, Springer US, Boston, MA, 1988, pp. 965–973, https://doi.org/10.1007/978-1-4684-6581-5_82.
[66] H. Wang, H. Li, F. Yan, Synthesis and mechanical properties of metakaolinite-based geopolymer, Colloids Surf. A Physicochem. Eng. Asp. 268 (1–3) (2005) 1–6, https://doi.org/10.1016/j.colsurfa.2005.01.016.
[67] T. Ding, J. Xiao, S. Zou, J. Yu, Flexural properties of 3D printed fibre-reinforced concrete with recycled sand, Construct. Build. Mater. 288 (2021), 123077, https://doi.org/10.1016/j.conbuildmat.2021.123077.
[68] T. Ding, J. Xiao, S. Zou, X. Zhou, Anisotropic behavior in bending of 3D printed concrete reinforced with fibers, Compos. Struct. 254 (2020), 112808, https://doi.org/10.1016/j.compstruct.2020.112808.
[69] G. Ma, Z. Li, L. Wang, G. Bai, Micro-cable reinforced geopolymer composite for extrusion-based 3D printing, Mater. Lett. 235 (2019) 144–147, https://doi.org/10.1016/j.matlet.2018.09.159.
[70] T. Marchment, J.G. Sanjayan, B. Nematollahi, M. Xia, Interlayer Strength of 3D Printed Concrete: Influencing Factors and Method of Enhancing, 3D Concrete Printing Technology, Elsevier, 2019, pp. 241–264, https://doi.org/10.1016/B978-0-12-815481-6.00012-9.
[71] V. Mechtcherine, V.N. Nerella, F. Will, M. Näther, J. Otto, M. Krause, Large-scale digital concrete construction – CONPrint3D concept for on-site, monolithic 3D-printing, Autom. ConStruct. 107 (2019), 102933, https://doi.org/10.1016/j.autcon.2019.102933.
[72] X. Chen, S. Wu, J. Zhou, Influence of porosity on compressive and tensile strength of cement mortar, Construct. Build. Mater. 40 (2013) 869–874, https://doi.org/10.1016/j.conbuildmat.2012.11.072.
[73] W. Lee, J. Van Deventer, The interface between natural siliceous aggregates and geopolymers, Cement Concr. Res. 34 (2) (2004) 195–206, https://doi.org/10.1016/S0008-8846(03)00250-3.
[74] J. Temuujin, A. van Riessen, K. MacKenzie, Preparation and characterisation of fly ash based geopolymer mortars, Construct. Build. Mater. 24 (10) (2010) 1906–1910, https://doi.org/10.1016/j.conbuildmat.2010.04.012.
[75] B. Panda, N.A. Noor Mohamed, Y.W.D. Tay, M.J. Tan, Bond strength in 3D printed geopolymer mortar, in: RILEM International Conference on Concrete and Digital Fabrication, Springer, 2018, pp. 200–206, https://doi.org/10.1007/978-3-319-99519-9_18.
[76] B. Panda, S.C. Paul, N.A.N. Mohamed, Y.W.D. Tay, M.J. Tan, Measurement of tensile bond strength of 3D printed geopolymer mortar, Measurement 113 (2018) 108–116, https://doi.org/10.1016/j.measurement.2017.08.051.
[77] Y.W.D. Tay, G.H.A. Ting, Y. Qian, B. Panda, L. He, M.J. Tan, Time gap effect on bond strength of 3D-printed concrete, Virtual Phys. Prototyp. 14 (1) (2019) 104–113, https://doi.org/10.1080/17452759.2018.1500420.